# Direct Measurement of the pH of Aerosol Particles using Carbon Quantum Dots

Emma C. Tackman, Rachel S. Grady[#], and Miriam Arak Freedman*

*Department of Chemistry, The Pennsylvania State University, University Park, PA 16802, USA*

*Manuscript in Preparation for Submission to Analytical Methods*
*June 9th, 2022*

*To whom all correspondence should be addressed: maf43@psu.edu, 814-867-4267
[#]Present address: Department of Chemistry, Villanova University, 800 Lancaster Avenue, Villanova, PA 19085, USA

## Abstract

The pH of aerosol particles remains challenging to measure because of their small size, complex composition, and high acidity. Acidity in aqueous aerosol particles, which are found abundantly in the atmosphere, impacts many chemical processes from reaction rates to cloud formation. Only one technique – pH paper – currently exists for directly determining the pH of aerosol particles, and this is restricted to measuring average acidity for entire particle populations. Other methods for evaluating aerosol pH include filter samples, particle-into-liquid sampling, Raman spectroscopy, organic dyes, and thermodynamic models, but these either operate in a higher pH range or are unable to assess certain chemical species or complexity. Here, we present a new method for determining acidity of individual particles and particle phases using carbon quantum dots as a novel in situ fluorophore. Carbon quantum dots are easily synthesized, shelf stable, and sensitive to pH in the highly acidic regime from pH 0 to pH 3 relevant to ambient aerosol particles. To establish the method, a calibration curve was formed from the ratiometric fluorescence intensity of aerosolized standard solutions with a correlation coefficient ($R^2$) of 0.99. Additionally, the pH of aerosol particles containing a complex organic mixture (COM) representative of environmental aerosols was also determined, proving the efficacy of using carbon quantum dots as pH-sensitive fluorophores for complex systems. The ability to directly

measure aerosol particle and phase acidity in the correct pH range can help parametrize atmospheric models and improve projections for other aerosol properties and their influence on health and climate.

**Introduction**

Atmospheric aerosol particles are known to be highly acidic, which has important implications for particle-phase chemistry in the environment. pH, a measure of the activity of the hydrogen cation in a solution, is a critical parameter to consider for aqueous aerosol systems and is defined by

$$\mathrm{pH} = -\log(\gamma_{H+}[H^+]) \quad (1)$$

where $\gamma_{H+}$ is the activity coefficient and $[H^+]$ is the concentration of protons. Particle acidity dictates the rates of gas partitioning for semivolatile compounds, changing the chemical composition of these liquid phases.[1–3] Condensation and growth of new, or secondary, aerosol particles from volatile compounds is enhanced on acidic seed particles with the acid-catalyzed formation of highly oxidized organics and organosulfates.[3–5] Additional heterogeneous processes such as metal dissolution and ice nucleation are known to be affected by the acidity of particles.[1,6,7] pH influences particle phase state by altering phase transitions based on the protonation state of organic acids present as well as the identities of soluble inorganic salts.[8–10] Because deprotonated acids are more soluble in salt solutions than their protonated counterparts, phase separation is less likely to occur and the relative humidity of phase separation is decreased in low acidity environments.[8,9,11] Collectively, these acid-derived effects on aerosol particle properties in turn have secondary and intermixed effects. For example, chemical content as determined by reactions and gas partitioning can change the morphology and toxicity of a particle, having implications for human health as well as the climate. Specifically, acidic aerosol

particles are hypothesized to be more toxic because of their increased ability to dissolve metals as well as penetrate into lung tissue and cause irritation due to their small size.[6,12] Also, high acidity levels in aqueous particles promote the formation of high molecular weight compounds through acid-catalyzed reactions.[13] These species tend to be surface active, which increases the overall particle's ability to act as a cloud condensation nucleus and promote cloud formation.[14] Clouds proximately impact Earth's climate as they are an antecedent for precipitation and also alter planetary albedo. Because of the ubiquity of atmospheric aerosol particles, experimentally determining with confidence the acidity of aerosol particles is critical for understanding physical and chemical processes in the environment.

Aerosol particle acidity is challenging to measure directly due to the small volume of the liquid phase in submicron particles which prevents the use of traditional pH measurements like glass bulb probes or titration. In the past, experimental measurements of aerosol pH have relied primarily on filter extractions to overcome volume limitations.[12,15,16] Filter extraction studies involve impacting ambient particles onto a filter substrate and transferring the collected materials into a known volume of solvent, usually water. Properties of the bulk extraction supernatant are then assessed and the pH of the original filter sample is back calculated.[15,17–19] Significant error can be associated with this back calculation arising from fundamental differences between extract and the particle liquid phase. Proton concentrations do not necessarily scale proportionally with dilution due to gas-phase buffering and the nonconservative extraction of species participating in weak acid equilibria.[15,16,18–22] Further, determining the liquid water content of the original filter sample is not straightforward, so predicting aerosol proton concentration can be a challenge.[1,16]

The particle-into-liquid sampler (PILS) is a notable improvement on the filter extraction method where humidified aerosol particles are collected through impaction into a liquid flow for immediate analysis. PILS was designed to prevent unwanted chemical processing due to gaseous species and extended periods between collection and evaluation.[16,23] However, this technique is still subject to the unwanted effects of liquid sample dilution seen with filter extractions.[16] Additionally, while both PILS and filter extract analysis frequently assesses the ion content of aerosol particles, the original ion activities of the species are not considered. pH deviates from simple proton concentration in nonideal solutions and aqueous particles are thought to be variable and highly concentrated and, therefore, far from ideal.[1,22,24,25] Neither external mixtures nor phase states are accounted for in PILS or filter samples, where populations of atmospheric aerosol particles are almost certainly not uniform and levels of acidity can vary between particles and from phase to phase.[10,26] For these reasons, thermodynamic modeling has been used to predict properties and behavior of atmospheric aerosol particles, including acidity.[2,15] Models offer the best predictions for particle acidity, but different modeling methods disagree on specific pH values for atmospheric aerosols based on differing priorities, sometimes overlooking important factors like organic components and nonideality.[12,20,22,24–26]

Because of the complications associated with proxy methods and modeling, some attention has been given to the direct measurement of aerosol particle acidity. Rindelaub et al. have used Raman spectra of lab-generated model aerosol particles to measure pH by the relative concentration of acid-conjugate base pairs, which provided quantitative results for particles containing no more than four species.[27] It is unclear if Raman can be used as systems increase in complexity.[28] Craig et al. were also able to evaluate aerosol particle acidity by impacting large quantities of aerosol onto pH paper in an experiment corollary to a filter collection. Using pH

paper as the substrate means that extraction into solvent is not necessary and particle acidity can be probed immediately upon impaction. This method is reliable in the low acidity regime of pH 3 to pH 6, but seems to show reduced sensitivity in the highly acidic, environmentally relevant range of pH 0 to pH 3.[29] Others have expanded on this paper-based technique, both modifying the way color responses are processed and applying the measurement for a select number of purposes.[25,30–32] These pH paper measurements, while improved, can still have a range of obstacles in determining pH and are limited to measuring the average pH of populations of impacted particles. Relatively large amounts of impacted liquid aerosol mass are required to illicit a color response from the color indicator paper and that color response is regularly nonuniform.[29,30,32] A variable color swatch is likely to occur due to unstable dyes, drying rates, or concentration gradients which introduce the need for subjective judgement when picking which shades to analyze.[25,31]

Recently, the use of fluorescence to measure the physicochemical properties of single atmospheric aerosol particles has been of some interest. A non-native internal fluorophore can be a useful tool in systematically measuring particle attributes in a controlled environment. Fluorescence measurements have the added advantage of assessing the pH of individual particles. The fluorescent dye Nile Red is solvatochromic, emitting at varying wavelengths depending on the polarity of the surrounding solution. Ohno et al. and Huang et al. exploited this property by incorporating Nile Red into model aerosol particles containing organic and inorganic components and using the fluorescence wavelengths emitted to infer separation of multiple liquid phases of differing polarities.[33,34] In a more germane study, Dallemagne et al. used Oregon Green 488, another fluorescent dye, to evaluate acidity and liquid-liquid phase separation in model aerosol particles composed of polyethylene glycol (PEG) and ammonium sulfate using a

ratiometric fluorescent response. Because the fluorophore sensor was an organic dye, it was preferentially soluble in the organic-rich PEG phase after phase separation, demonstrating potential for measuring acidity in the individual phases of a phase separated particle depending on the solubility of the fluorophore. Unfortunately, the $pK_a$ of Oregon Green 488 is 4.6 which limits its linear response to roughly pH 3 to 6, excluding the atmospherically relevant target pH range.

Quantum dots are fluorescent nanoparticles typically less than 10 nm in size which are here proposed to be a good alternative pH-sensitive fluorophore for atmospheric applications because of their high stability and tunable optical and chemical properties. The optical and electronic properties of quantum dots are extremely dependent on size and composition which facilitates tunability via varying synthesis conditions.[35] Carbon-based quantum dots are becoming a topic of interest as they are easy to synthesize, environmentally friendly, and nontoxic. Additionally, they are preferable to fluorescent dyes as they are shelf stable and typically do not photobleach.[36–40] Carbon dots are nanomaterials composed of $sp^2$ or $sp^3$ hybridized carbon with physical structures increasing in complexity in a number of ways: with multiple layers in a stacked configuration like graphite, higher disorder, or with the introduction of heteroatoms. Oxygen-containing surface functional groups like ethers, alcohols, and carboxylic acids help to stabilize the dots in aqueous environments.[41] Also, heteroatoms such as nitrogen incorporated into the carbon dot structure have been shown to boost the quantum yield of the resulting fluorophore.[42–44] Both graphene edges and surface functional groups can introduce electronic states into the intrinsic band gap of the carbon core, creating lower energy transitions. Indeed, it has been shown that, for carbon dots of the same size, dots whose surfaces have been more oxidized display red-shifted fluorescence.[36,37,45,46] Blue fluorescence is the most

common for carbon quantum dots as wavelengths in this range correspond to the energy of the $\pi$-$\pi^*$ transition of $sp^2$ hybridized carbon domains.[37,47] By introducing surface or edge states, also known as defect states, carbon dots that fluoresce at every visible color can be achieved.[47] Surface passivation or functionalization can also provide a mechanism for tuning the solubility of carbon quantum dots, allowing for extended use of these fluorophores in both aqueous and organic rich environments.[41]

In this paper, we use carbon quantum dots with pH-dependent ratiometric fluorescence as an internal fluorophore to measure the level of acidity in individual aerosol particles of known composition. Carbon quantum dots have the benefit of being exceptionally easy to synthesize from small molecule precursors and are sensitive under highly acidic conditions, unlike other possible organic fluorescent molecules.[48] We demonstrate that our synthesized carbon dots are advantageously responsive to pH, both in bulk and in supermicron aerosol particles, and are preferentially soluble in the organic phase of a binary particle after phase separation. For aerosol measurements, a ratiometric approach was taken to avoid the influences of fluctuations in fluorescence intensity due to concentration. Using the ratio of integrated emission intensity at two excitation wavelengths facilitates a concentration-independent measurement, so the accumulation or dilution of fluorophores will not influence the assessment of particle pH.[10,49] We further show that carbon dots are compatible with aerosol particles comprised of a complex mixture of organic compounds which serves as a proxy for the chemical composition of atmospheric aerosol. The pH of this model system was successfully measured using the variable fluorescence exhibited by carbon dots. The novel application of carbon quantum dots in aerosol particles has the potential to be a useful tool toward stable single particle acidity measurements and further, toward an improved understanding of the atmospheric chemical system.

**Methods**

Carbon quantum dots were synthesized according to a modified version of the method reported by Qu et al.[50] 3 g of citric acid (≥99.5%, Sigma-Aldrich) were combined with 3 g of urea (99%, Sigma-Aldrich) in 10 mL of HPLC-grade water (Fisher Scientific). This solution was microwaved for 5 minutes in a 700-watt domestic microwave oven (Hamilton Beach). The resulting black solid was reconstituted in two 30 mL aliquots of water and centrifuged at 8000 rpm for 12 hours. The supernatant suspension containing the carbon dot product was carefully collected and stored in a refrigerator, discarding the remaining solid brown residue. Reaction yields are difficult to gauge and are not reported here because some amount of precursor was not converted to carbon dots but instead left as a solid residue. However, because the fluorescence response is ultimately considered ratiometrically, the experiment does not require exact quantum dot concentrations. Aliquots of the supernatant stock solution were brought to room temperature and diluted to trace amounts (about 1:400) for characterization and fluorescence experiments and, despite ambiguous reaction yields, the synthesis was found to be highly repeatable (Table S1a). A pH meter (SevenCompact, Mettler Toledo) with an accuracy of ±0.002 pH units was used to assess the pH of samples and solutions.

Standard and reference solutions were composed of hydrochloric acid (99.999%, Alfa Aesar), sulfuric acid (GR ACS, EMD), ammonium sulfate (>99%, Sigma-Aldrich), 2-methylglutaric acid (98%, Alfa Aesar), sucrose (>99%, Fisher Scientific,) and quinine sulfate (>99%, Ward's Scientific). Absorbance measurements were made on a UV-vis-NIR spectrophotometer (Lambda 950, Perkin-Elmer). A fluorescence spectrophotometer (Varian Cary Eclipse, Agilent) was used for emission and excitation measurements. For initial fluorometer experiments, samples were prepared by diluting the carbon dot stock with HPLC-grade water or

hydrochloric acid solutions of varying concentrations, which were analyzed immediately after preparation. Any strong inorganic acid could be used to make up these standard solutions. A Zetasizer Nano ZS (Malvern) was used for dynamic light scattering (DLS) measurements. 2μL of a dilute carbon quantum dot solution (1:500) was drop cast onto a copper-supported carbon transmission electron microscope (TEM) substrate (Electron Microscopy Sciences) and analyzed using a Talos F200C transmission electron microscope (FEI). An aliquot of the concentrated solution was allowed to sit under a nitrogen stream until dry, which produced a fine black powder. This powder sample was used for Fourier transform infrared (FT-IR) spectroscopic analysis (Vertex 80, Bruker) and X-ray photoelectron spectroscopy (VersaProbeII, Physical Electronics).

For optical and fluorescence microscope experiments, sample solutions were again prepared by diluting the carbon dot stock to trace concentrations (about 1:400) with HPLC-grade water or aqueous solutions of varying composition (see below). Supermicron aerosol particles were produced by spraying solutions onto hydrophobic glass microscope slides, generating particles about 10 to 1000 μm in diameter.[8,9] Particles between 10 and 200 μm were selected for analysis. Sample slides were placed into an environmental chamber on the microscope stage in which the relative humidity (RH) around the particles was regulated through the controlled flow of dry and humidified nitrogen.[9] The RH within the environmental chamber could be modulated from less than 2% RH to greater than 95% RH, although the usefulness of the setup for pH measurement at very low RH values is not straightforward as the pH of a system becomes irrelevant due to lack of free protons at very low water content. The RH in the chamber was measured using a humidity probe (HMP60, Vaisala). For experiments measuring the RH of phase transitions, the chamber RH was ramped at ≤1% RH per minute, a rate sufficiently slow

for equilibration between the gas flow and liquid particle phases.[9] For fluorescence measurements, particles were rapidly equilibrated by decreasing the RH to ≤ 20% RH and then raising it to ≥90% RH and holding for at least 20 minutes before taking a measurement. Although the level of acidity is expected to be maintained through the aerosolization process from bulk to particle, solutions were buffered where possible.[9,10] Bulk solutions were prepared from pH 0.5 to pH 3 at approximately 0.5 pH unit increments. 0.3M solutions of sodium phosphate monobasic (>99%, Dot Scientific Inc.) and sodium phosphate dibasic (>99%, Dot Scientific Inc.) were used to buffer samples between pH 2.03 and pH 3.02 while those from pH 0.54 to pH 1.61 were made from unbuffered sulfuric acid. All fluorescence microscope samples were also composed of 5 wt% sucrose to prevent rapid water loss from evaporation. A complex organic mixture (COM) modified from one defined by Song et al. was used as a proxy for ambient aerosol (Table S2).[51] Buffers, acids, sucrose, and COM were all confirmed to not produce fluorescence independent of the carbon dot fluorophore. Also, no shift in the fluorescence of the quantum dots was observed in the presence of these components (Table S1b).

**Results and Discussion**

A pH-sensitive carbon-based quantum dot fluorophore was synthesized using citric acid and urea as small molecule precursors. The fluorescence emission spectra for the carbon quantum dots matched well with literature for the same synthesis conditions demonstrating successful formation of the desired product (Fig. 1).[50] Citric acid was chosen as a readily available carbon and oxygen source and urea as a nitrogen source. Neither of these precursors fluoresce, so the source of any fluorescence in the synthesis product is reasonably attributed to the formation of carbon quantum dots.[50] The carbon dot absorption spectrum displays a peak at 340 nm, characteristic of a highly aromatic carbon system, as well as another at 400 nm (Fig.

S1).[36,50] The second absorption band arises from defects within the carbon structure of the quantum dot. Possible defects include the boundary between $sp^2$ and $sp^3$ hybridized nanodomains and the inclusion of oxygen- and nitrogen-containing functional groups.[36] The wavelength of fluorescence for these carbon dots was found to be excitation wavelength-dependent, with emission peaks broadening and red shifting with increasing excitation wavelengths (Fig. 1). This phenomenon is commonly observed for carbon-based fluorescent material and, although not fully understood, might be a result of polydispersity in quantum dot size as well as the large variety of active "emissive sites" including edge structure and surface functional groups.[36,37,39,43–45,50,52,53] The two prominent peaks in Figure 1 have maxima at 460 nm and 525 nm, corresponding to excitation wavelengths of 350 nm and 405 nm respectively. The presence of energetically distinct maxima suggests at least two fluorescence mechanisms contributing to the overall emission of the carbon dot system, although it is likely that many different yet complementary components make up each peak.[37] The peak at 465 nm is hypothesized to be associated with an ordered carbon core while the peak at 525 nm might be related to

heterodispersity in size or the presence of heteroatoms introduced to the system by the precursors.[36,45,47,50]

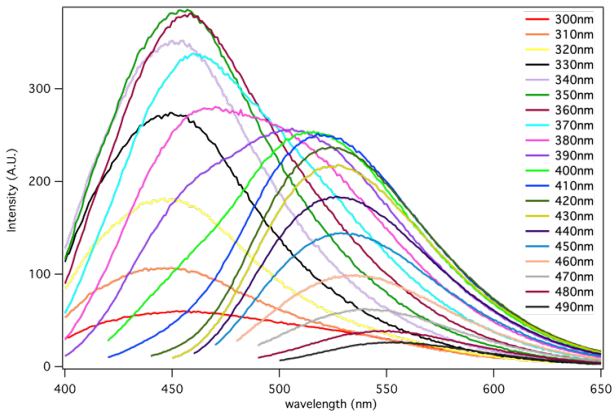


**Figure 1.** Fluorescence emission for synthesized carbon quantum dots is dependent on excitation wavelength and displays two major peaks. Fluorescence spectra were recorded at 300 nm to 490 nm excitation in 10 nm increments. The excitation wavelength is given in the legend with the corresponding emission spectrum shown in the figure.

DLS measurements were used to assist in determining the hydrodynamic diameter of the synthesized carbon dots as an approximation of actual particle diameter. These results were inconclusive, suggesting a high level of diversity present in the synthesis products, contrary to the literature product of 1-4 nm carbon spheres.[50] It is hypothesized that the domestic microwave oven may provide inconsistent sample irradiation or slow ramp times which could lead to high polydispersity in the quantum dot product. In contrast, TEM images suggest that the carbon dots were generally round and monodisperse with a mean diameter of 7.6 nm ± 1.8 nm (Fig. S2). Deviations from literature may again arise from differences in microwave instrumentation. XPS results showed an increase in the number of carbons present in the carbon dot product relative to the precursors (Fig. S3). Primary elements observed were carbon, oxygen, and nitrogen, with carbon present in the highest abundance. This result was expected based on the identity of the precursors. No other elements or bonding environments were found, suggesting that significant

contamination was unlikely. The broad, symmetrical $CH_x$ peak (Fig. S3d) suggests a carbon structure that is more amorphous than graphitic. This result is supported in the FT-IR spectrum, which shows distinct vibrational modes which would be indistinguishable for a heavily graphitized carbon product (Fig. S4a), although some graphite-like character is still expected. Additionally, vibrational modes for the carbon dot product exist that do not appear in the FT-IR spectra for the precursor molecules, implying that a distinct product has been successfully fabricated (Fig. S4b,c).

Our synthesized carbon dots were found to give relatively intense fluorescence. The quantum yield of the most intense peak ($\lambda_{ex}$ 350 nm) was measured at 12.4%, which is well-matched with the literature value of about 13% (Fig. S5).[40,50] Our quantum yield is appreciably higher than many other carbon quantum dot products found in literature, typically between 1-6%, although this value can be increased with surface passivation and the presence of heteroatoms.[37,52,54] To test the temporal stability of the carbon dot product, a fluorescence spectrum of that same peak ($\lambda_{ex}$ 350 nm) was acquired once every week for seven weeks, where a fresh dilution (1:400) was prepared each week (Fig. S6a). Peak intensity remained markedly stable across this time period, confirming that the concentrated carbon dots synthesized here were shelf-stable on a time scale of months. An analogous experiment was conducted for a solution of dilute carbon dots (1:400) in HCl at pH 3, where the same solution was sampled once per week for seven weeks. The fluorescence intensity for this solution was diminished by about 15%, implying that the product, while typically stable, will degrade slightly under acidic conditions (Fig S6b).

The pH responsiveness of these carbon quantum dots was characterized by diluting the dots with various concentrations of hydrochloric acid. Fluorescence was found to decrease

monotonically with increasing acidity below pH 3.5 (Fig. 2). Above this value, carbon dot fluorescence remained steady in the low acidity regime. The response of the carbon dot fluorescence intensity to pH could be explained by the reversible protonation or deprotonation of functional groups containing oxygen and nitrogen at the surface of the carbon dot. Changes in surface chemistry alter the electronic structure of the system which can possibly lead to reduced fluorescence intensity by introducing new nonradiative relaxation pathways depending on the pH of their surroundings.[36,40,43] If all surface groups that can be deprotonated have been deprotonated, then the dynamic response of the fluorophores to pH will diminish, as we suggest is the case above pH 3.5 for the carbon quantum dots studied here. Figure 2a also shows a slight blue shift in the 425 nm peak maximum with increasing acidity, again possibly driven by altered electronic band structure as a consequence of changes in surface chemistry.[36]

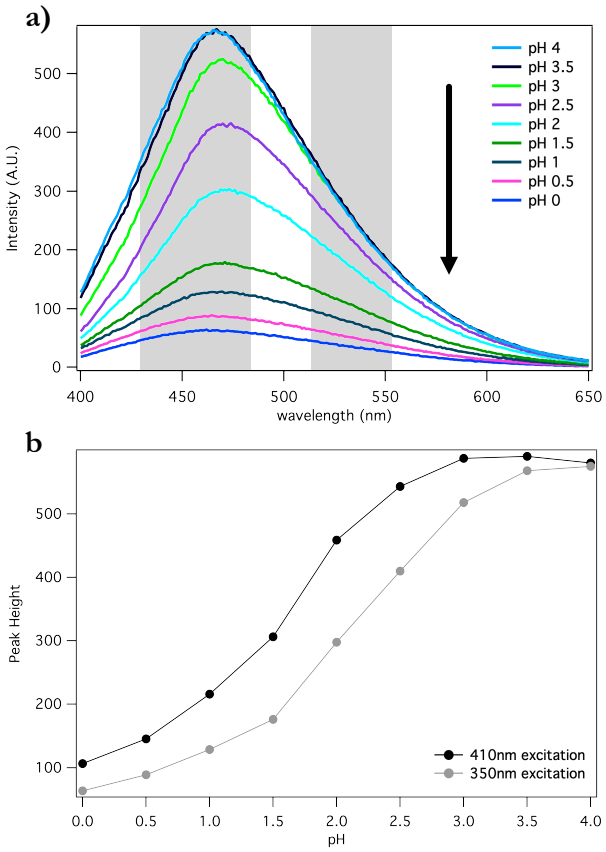


**Figure 2. a)** Synthesized carbon quantum dot emission spectra ($\lambda_{ex}$ 350 nm) show decreasing fluorescence intensity with increasing acidity. Shaded regions represent the emission wavelengths that will be used for quantitative analysis. **b)** Peak height for both emission maxima ($\lambda_{ex}$ 350 nm and $\lambda_{ex}$ 410 nm) versus pH show excellent sensitivity to acidity in the environmentally relevant range of pH 0 to pH 3. Fluorescence response quickly levels off for both peaks above pH 3.5.

Carbon quantum dots were incorporated into model aerosol particles to be used an in situ fluorescent pH sensor. Although present in scant amounts relative to the other components, it was necessary to ensure that the carbon dot fluorophores did not influence the relevant inherent thermodynamic properties of the systems to which they are applied. To test this, carbon dots were added to previously characterized inorganic/organic model aerosol particles composed of

ammonium sulfate and 2-methylglutaric acid in a 1:1 ratio at 5 wt% total (Fig. 3). The appropriate properties here were the relative humidities at which phase transitions occur, which were measured in the absence and presence of the carbon dot fluorophores. Previous work without carbon dots show that aerosol particles of this composition undergo liquid-liquid phase separation at 79.4 ± 1.0% RH, efflorescence at 40.6 ± 3.9% RH, and deliquescence at 81.2 ± 1.1% RH.[9] The same experiment was repeated in the presence of carbon dots and the relative humidities of phase transitions were found to be essentially identical at 80.2 ± 0.6% for liquid-liquid phase separation, 38.0 ± 3.5% RH for efflorescence, and 82.8 ± 0.4% for deliquescence, where the difference between the two sets of values falls within the error of the instrumentation. Figure 3 shows that the carbon dots accumulated in the outer organic phase of the phase separated particle, indicated by the uniform fluorescence throughout the well mixed particle at high RHs and the absence of fluorescence in the inner phase after separation at low RHs. Because the RHs for phase transitions for particles composed of this binary mixture are maintained, these data confirm that the set of carbon quantum dots synthesized using the above method can be used for in situ measurements of aerosol particle acidity without altering the phase transition properties of the model aerosol system.

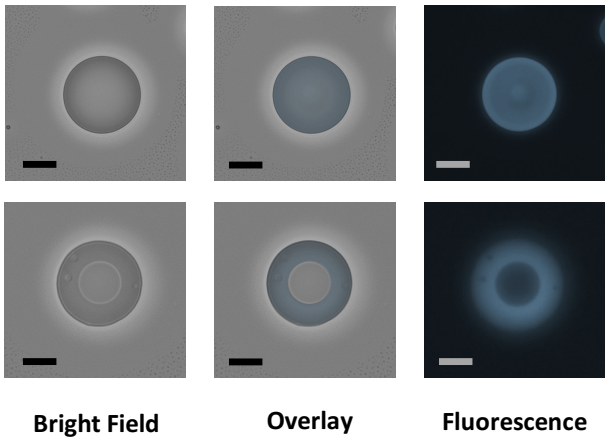


**Figure 3.** Homogeneous (top) and phase separated (bottom) organic/inorganic model aerosol particles containing carbon quantum dots under bright field (left) and fluorescence (right, false color) with the overlay of the two (center). Carbon dot fluorophores are preferentially soluble in the organic outer phase when present at RHs below the separation relative humidity. Fluorescence at $\lambda_{ex,361\text{-}389}$/ $\lambda_{em,435\text{-}485}$. All scale bars 10 μm. Figure format based on Fig. 2 from Ref. 10.

The fluorescence of our synthesized carbon quantum dots was established to have a positive relationship with pH via fluorescence spectroscopy, but because fluorescence intensity is proportional to the concentration of fluorophores, it is challenging to achieve reliable and quantifiable results using emission peak height or area alone for application in model aerosol microparticles. The size and water content of particles, and thus fluorophore concentration, fluctuates with relative humidity. A ratiometric method can be used to overcome this, where some portion of the fluorescence spectrum is normalized to another; all else being equal, the ratio of these spectral regions should be the same for all fluorophore concentrations, meaning that concentration-independent fluorescence response can be measured.[10,47,49,55] Here, fluorescence microscope studies employ filter cubes to isolate the grayed regions of the fluorescence spectrum shown in Figure 2a. A filter cube is an optic in a fluorescence microscope setup used to set

excitation and emission windows. Images captured by a CCD camera detector in the optical microscope setup are composed of the integrated intensity of each gray region across a select band of excitation wavelengths. These wavelengths are used in ratio to measure particle acidity, as the area under the curve for each region changes at different relative magnitudes with varying pH (Fig. 2b). For example, Figure 2b shows the pH dependence of two peak maxima corresponding to two different excitation wavelengths for the carbon dots synthesized here. The respective fluorescence intensities of these maxima will vary with fluorophore concentration but the ratio of the two will not. The responses to pH at these wavelengths differ, forming the basis for the ratiometric measurement. Again, the exact emission wavelengths used in ratio in this experiment are shown in gray in Figure 2a. The precise wavelengths used for analysis in this experiment were chosen primarily based on the filter cubes that were available. The only requirements for wavelength selection are that the quantum dots substantially emit in the chosen spectral regions and that the two regions to be used for ratiometric analysis do not overlap. It is also worth noting that the pH dependence of the carbon dot fluorophores found using single wavelength fluorometer measurements (Fig. 2b) should correspond closely to the dependence as seen using a fluorescence microscope (Fig. 4), but direct comparisons are not appropriate. Because the filter cubes in a fluorescence microscope excite across a range of excitation wavelengths, integration is done beneath an emission "surface" rather than an emission curve. The surface integrations for the fluorescence microscopy measurements are difficult to predict using a fluorometer as each spectrum given by a fluorometer corresponds to a single excitation wavelength. Extrapolation between these fluorometer spectra is necessary to recreate the total emission surface, which is not easily achievable to a reasonable degree of accuracy.

Figure 4 shows that the synthesized carbon quantum dots are sensitive to pH in highly acidic environments with decreasing ratiometric fluorescence intensity from pH 3 down to pH 0.5. For each point, the total fluorescence intensity measured at $\lambda_{ex,\ 361\text{-}389}/\ \lambda_{em,\ 515\text{-}555}$ was divided by the intensity at $\lambda_{ex,\ 465\text{-}495}/\ \lambda_{em,\ 577\text{-}632}$ and the resulting value, while fluorophore concentration-independent, was found to depend monotonically on the pH of the medium. The calibration curve constructed from measuring aerosol particles of known pH showed that the ratiometric fluorescence intensity of the carbon dots was decisively correlated to particle pH with an $R^2$ of 0.99 for a trinomial fit (Fig.4). This calibration curve used to assess the acidity of particles generated from a solution containing 9 organic compounds (Table S1). These species, when used together as in previous work by Song et al. and others, are an example of a COM.[51,56] COM are mixtures meant to represent the diversity of organic compounds found in ambient aerosol particles, e.g., dicarboxylic acids, aromatic compounds, and polyols. In bulk, the pH of the COM solution was measured at 1.87. Atmospheric proxy aerosol particles containing COM were made in the same manner as the standard solutions using a spray bottle to generate droplets. Fluorescence intensity for these droplets was measured at the same wavelengths as the standard and used in ratio in the standard calibration curve. The fluorescence-based pH measurement for aerosol particles generated from this mixture was found to be very close to the bulk value at pH 1.89 ± 0.03. The difference between the two values falls within error of the measurement. The successful determination of the pH of proxy aerosol particles composed of environmentally relevant compounds here demonstrates the feasibility of applying this new analytical system as an indicator of aerosol particle acidity.

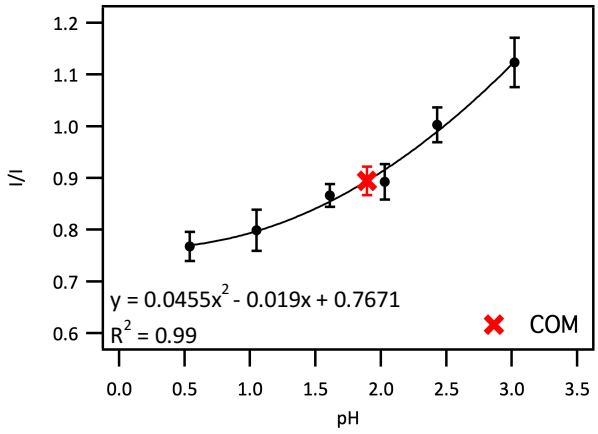


**Figure 4.** Ratio of the fluorescence intensities of $\boldsymbol{\lambda}_{ex,\ 361\text{-}389}/\ \boldsymbol{\lambda}_{em,\ 515\text{-}555}$ to $\boldsymbol{\lambda}_{ex,\ 465\text{-}495}/\ \boldsymbol{\lambda}_{em,\ 577\text{-}632}$ vs pH. This relationship was used to determine the pH of a COM mixture denoted by the symbol in red. The bulk pH of the COM solution was 1.87 and the pH of the aerosols produced from this mixture was found to be in good agreement at 1.89 ± 0.03.

## Conclusions

Carbon quantum dots are an ideal fluorophore for chemical environments comparable to those found in the liquid phase of ambient aerosol particles due to their high stability as well as sensitivity to pH under highly acidic conditions. Carbon dots were used here as a novel fluorophore for probing the acidity of laboratory generated model aerosol particles in situ and were shown to be advantageous over existing techniques as they have the potential for further investigations of acidity at an atmospherically relevant pH range and in individual particle phases. Carbon dots are a good candidate for this assay as they are easy to produce from readily available precursors and exhibit stable fluorescence for months after synthesis. Here, acidified particles in the range of pH 0.5 – 3 were used to establish the relationship between a ratio of carbon dot emission wavelengths and aerosol particle acidity. The pH of particles consisting of an atmospherically relevant organic mixture was tested using this relationship, which was found

to be consistent with the pH of the particles' bulk solution counterpart meaning that this probe can be used to assess acidity in chemically complex conditions.

These promising results demonstrate the potential for our fluorescent probe as a new method for the direct determination of aerosol acidity. Carbon quantum dots could aid in overcoming many of the problems associated with indirect pH measurements and modeling for supermicron aerosol particles. The composition of carbon dots determines their fluorescence mechanisms and ultimately their specific sensitivities. Carbon dots with alternative sensitivities such as a dynamic response to level acidity in a range of pH values beyond those outlined in this study could be fabricated. More factors have yet to be considered in the direct application of fluorescent probes to ambient aerosols, including accounting for the autofluorescence of many aromatic compounds found in secondary organic material.[57] The improved ability to measure liquid aerosol pH betters our understanding of the interconnected physicochemical properties of aerosol particles and by extension the parametrization of thermodynamic models predicting the impacts of aerosol particles on health and climate.

**Associated Content**

Supporting Information: supplemental experimental details including complex organic mixture composition. Further images and descriptions of carbon quantum dot probe characterization.

**Author Information:**

**Corresponding Author**
*To whom correspondence may be addressed. Email: maf43@psu.edu, 814-867-4267

**Notes**
The authors declare no competing interest.

**Acknowledgement**

This work was supported by the National Science Foundation (NSF CAREER Award CHE-1351383, NSF CHE-1904803, NSF AGS-1916758). The authors thank J. Shallenberger and TJ Zimudzi for help with characterization as well as E. Garbioglu and L. Collazo Perez for auxiliary contributions. We also thank Q. Huang for helpful discussions.

**References:**

1 H. Guo, L. Xu, A. Bougiatioti, K. M. Cerully, S. L. Capps, J. R. Hite Jr., A. G. Carlton, S.-H. Lee, M. H. Bergin, N. L. Ng, A. Nenes and R. J. Weber, *Atmos. Chem. Phys.*, 2015, **15**, 5211–5228.
2 Y. Chen, H. Shen and A. G. Russell, *Environ. Sci. Technol.*, 2019, **53**, 9646–9655.
3 Y. Zhang, Y. Chen, Z. Lei, N. E. Olson, M. Riva, A. R. Koss, Z. Zhang, A. Gold, J. T. Jayne, D. R. Worsnop, T. B. Onasch, J. H. Kroll, B. J. Turpin, A. P. Ault and J. D. Surratt, *ACS Earth Space Chem.*, 2019, **3**, 2646–2658.
4 M. Jang, N. M. Czoschke, S. Lee and R. M. Kamens, *Science*, 2002, **298**, 814–817.
5 Y. Iinuma, O. Böge, T. Gnauk and H. Herrmann, *Atmos. Environ.*, 2004, **38**, 761–773.
6 T. Fang, H. Guo, L. Zeng, V. Verma, A. Nenes and R. J. Weber, *Environ. Sci. Technol.*, 2017, **51**, 2611–2620.
7 O. Möhler, S. Büttner, C. Linke, M. Schnaiter, H. Saathoff, O. Stetzer, R. Wagner, M. Krämer, A. Mangold, V. Ebert and U. Schurath, *J. Geophys. Res. Atmos.*, , DOI:10.1029/2004JD005169.
8 D. J. Losey, R. G. Parker and M. A. Freedman, *J. Phys. Chem. Lett.*, 2016, **7**, 3861–3865.
9 D. J. Losey, E.-J. E. Ott and M. A. Freedman, *J. Phys. Chem. A*, 2018, **122**, 3819–3828.
10 M. A. Dallemagne, X. Y. Huang and N. C. Eddingsaas, *J. Phys. Chem. A*, 2016, **120**, 2868–2876.
11 E.-J. E. Ott, E. C. Tackman and M. A. Freedman, *ACS Earth Space Chem.*, 2020, **4**, 591–601.
12 M. A. Freedman, E.-J. E. Ott and K. E. Marak, *J. Phys. Chem. A*, 2019, **123**, 1275–1284.
13 M. Hallquist, J. C. Wenger, U. Baltensperger, Y. Rudich, D. Simpson, M. Claeys, J. Dommen, N. M. Donahue, C. George, A. H. Goldstein, J. F. Hamilton, H. Herrmann, T. Hoffmann, Y. Iinuma, M. Jang, M. E. Jenkin, J. L. Jimenez, A. Kiendler-Scharr, W. Maenhaut, G. McFiggans, T. F. Mentel, A. Monod, A. S. H. Prévôt, J. H. Seinfeld, J. D. Surratt, R. Szmigielski and J. Wildt, *Atmos. Chem. Phys.*, 2009, **9**, 5155–5236.
14 Z. Li, A. L. Williams and M. J. Rood, *J. Atmos. Sci.*, 1998, **55**, 1859–1866.
15 C. J. Hennigan, J. Izumi, A. P. Sullivan, R. J. Weber and A. Nenes, *Atmos. Chem. Phys.*, 2015, **15**, 2775–2790.
16 J. Xue, A. K. H. Lau and J. Z. Yu, *Atmos. Environ.*, 2011, **45**, 7081–7088.
17 C. A. Alves, *Anais da Academia Brasileira de Ciências*, 2008, **80**, 21–82.
18 R. L. Tanner, in *Measurement Challenges in Atmospheric Chemistry*, American Chemical Society, 1993, vol. 232, pp. 229–241.
19 B. A. Nault, P. Campuzano-Jost, D. A. Day, H. Guo, D. S. Jo, A. V. Handschy, D. Pagonis, J. C. Schroder, M. K. Schueneman, M. J. Cubison, J. E. Dibb, A. Hodzic, W. Hu, B. B. Palm and J. L. Jimenez, *Atmos. Meas. Tech.*, 2020, **13**, 6193–6213.
20 A. Madhu, Z. Yu and M. Jang, *Aerosol Sci. Technol.*, 2021, **55**, 795–804.

21 G. Zheng, H. Su, S. Wang, M. O. Andreae, U. Pöschl and Y. Cheng, *Science*, 2020, **369**, 1374–1377.
22 S. Jia, X. Wang, Q. Zhang, S. Sarkar, L. Wu, M. Huang, J. Zhang and L. Yang, *Atmos. Chem. Phys.*, 2018, **18**, 11125–11133.
23 F. Drewnick, J. J. Schwab, O. Hogrefe, S. Peters, L. Husain, D. Diamond, R. Weber and K. L. Demerjian, *Atmos. Environ.*, 2003, **37**, 3335–3350.
24 X. Peng, P. Vasilakos, A. Nenes, G. Shi, Y. Qian, X. Shi, Z. Xiao, K. Chen, Y. Feng and A. G. Russell, *Environ. Sci. Technol.*, 2019, **53**, 8903–8913.
25 K. Gong, R. R. Jones, K. Li, G. Xu, F. Yiqing, V. K. Valev and L. Zhang, *Sensors and Actuators B: Chemical*, 2021, **346**, 130521.
26 M. A. Battaglia Jr., R. J. Weber, A. Nenes and C. J. Hennigan, *Atmos. Chem. Phys.*, 2019, **19**, 14607–14620.
27 J. D. Rindelaub, R. L. Craig, L. Nandy, A. L. Bondy, C. S. Dutcher, P. B. Shepson and A. P. Ault, *J. Phys. Chem. A*, 2016, **120**, 911–917.
28 H. C. Boyer, K. Gorkowski and R. C. Sullivan, *Anal. Chem.*, 2020, **92**, 1089–1096.
29 R. L. Craig, P. K. Peterson, L. Nandy, Z. Lei, M. A. Hossain, S. Camarena, R. A. Dodson, R. D. Cook, C. S. Dutcher and A. P. Ault, *Anal. Chem.*, 2018, **90**, 11232–11239.
30 G. Li, H. Su, N. Ma, G. Zheng, U. Kuhn, M. Li, T. Klimach, U. Pöschl and Y. Cheng, *Atmos. Meas. Tech.*, 2020, **13**, 6053–6065.
31 Q. Song and K. Osada, *Atmos. Environ.*, 2021, **261**, 118605.
32 K. J. Angle, D. R. Crocker, R. M. C. Simpson, K. J. Mayer, L. A. Garofalo, A. N. Moore, S. L. M. Garcia, V. W. Or, S. Srinivasan, M. Farhan, J. S. Sauer, C. Lee, M. A. Pothier, D. K. Farmer, T. R. Martz, T. H. Bertram, C. D. Cappa, K. A. Prather and V. H. Grassian, *PNAS*, , DOI:10.1073/pnas.2018397118.
33 P. E. Ohno, Y. Qin, J. Ye, J. Wang, A. K. Bertram and S. T. Martin, *ACS Earth Space Chem.*, 2021, **5**, 1223–1232.
34 Y. Huang, F. Mahrt, S. Xu, M. Shiraiwa, A. Zuend and A. K. Bertram, *PNAS*, , DOI:10.1073/pnas.2102512118.
35 D. Bera, L. Qian, T.-K. Tseng, P. H. Holloway, D. Bera, L. Qian, T.-K. Tseng and P. H. Holloway, *Materials*, 2010, **3**, 2260–2345.
36 M. Yang, B. Li, K. Zhong and Y. Lu, *J. Mater. Sci.*, 2018, **53**, 2424–2433.
37 S. Zhu, Y. Song, X. Zhao, J. Shao, J. Zhang and B. Yang, *Nano Res.*, 2015, **8**, 355–381.
38 Z. Yang, Z. Li, M. Xu, Y. Ma, J. Zhang, Y. Su, F. Gao, H. Wei and L. Zhang, *Nano-Micro Lett.*, 2013, **5**, 247–259.
39 A. Jaiswal, S. Sankar Ghosh and A. Chattopadhyay, *Chemical Communications*, 2012, **48**, 407–409.
40 D. Stefanakis, A. Philippidis, L. Sygellou, F. George, D. Ghanotakis and D. Anglos, *J. Nanoparticle Res.*, 2014, **16**, 2646.
41 P. Zhao and L. Zhu, *Chem. Commun.*, 2018, **54**, 5401–5406.
42 F. Ehrat, S. Bhattacharyya, J. Schneider, A. Löf, R. Wyrwich, A. L. Rogach, J. K. Stolarczyk, A. S. Urban and J. Feldmann, *Nano Lett.*, 2017, **17**, 7710–7716.
43 Z. Lian Wu, M. Xuan Gao, T. Ting Wang, X. Yan Wan, L. Ling Zheng and C. Zhi Huang, *Nanoscale*, 2014, **6**, 3868–3874.
44 X. Chen, Q. Jin, L. Wu, C. Tung and X. Tang, *Angew. Chem. Int. Ed.*, 2014, **53**, 12542–12547.

45 L. Bao, Z.-L. Zhang, Z.-Q. Tian, L. Zhang, C. Liu, Y. Lin, B. Qi and D.-W. Pang, *Advanced Materials*, 2011, **23**, 5801–5806.
46 M. L. Liu, B. B. Chen, C. M. Li and C. Z. Huang, *Green Chem.*, 2019, **21**, 449–471.
47 H. Nie, M. Li, Q. Li, S. Liang, Y. Tan, L. Sheng, W. Shi and S. X.-A. Zhang, *Chem. Mater.*, 2014, **26**, 3104–3112.
48 W. Niu, L. Fan, M. Nan, M. S. Wong, S. Shuang and C. Dong, *Sensors and Actuators B: Chemical*, 2016, **234**, 534–540.
49 J. Shangguan, D. He, X. He, K. Wang, F. Xu, J. Liu, J. Tang, X. Yang and J. Huang, *Anal. Chem.*, 2016, **88**, 7837–7843.
50 S. Qu, X. Wang, Q. Lu, X. Liu and L. Wang, *Angew. Chem. Int. Ed.*, 2012, **51**, 12215–12218.
51 M. Song, C. Marcolli, U. K. Krieger, A. Zuend and T. Peter, *Geophys. Res. Lett.*, , DOI:https://doi.org/10.1029/2012GL052807.
52 H. Zhu, X. Wang, Y. Li, Z. Wang, F. Yang and X. Yang, *Chem. Commun.*, 2009, 5118–5120.
53 Y. Liu, C. Liu and Z. Zhang, *J. Colloid Interface Sci.*, 2011, **356**, 416–421.
54 S. Ying Lim, W. Shen and Z. Gao, *Chemical Society Reviews*, 2015, **44**, 362–381.
55 J. Zuo, T. Jiang, X. Zhao, X. Xiong, S. Xiao and Z. Zhu, *J. Nanomater.*, , DOI:10.1155/2015/787862.
56 T. M. Kucinski, J. N. Dawson and M. A. Freedman, *J. Phys. Chem. Lett.*, 2019, **10**, 6915–6920.
57 Y. You, L. Renbaum-Wolff, M. Carreras-Sospedra, S. J. Hanna, N. Hiranuma, S. Kamal, M. L. Smith, X. Zhang, R. J. Weber, J. E. Shilling, D. Dabdub, S. T. Martin and A. K. Bertram, *PNAS*, 2012, **109**, 13188–13193.